


## Review

# Recent Progresses on Vanadium Sulfide Cathodes for Aqueous Zinc-Ion Batteries

Enze Hu, Huifang Li \*, Yizhou Zhang, Xiaojun Wang \* and Zhiming Liu \* 

Shandong Engineering Laboratory for Preparation and Application of High-Performance Carbon-Materials,  
College of Electromechanical Engineering, Qingdao University of Science & Technology, Qingdao 266061, China

\* Correspondence: huifang0801@gmail.com (H.L.); wangxiaojunchem@163.com (X.W.); zmlu@qust.edu.cn (Z.L.)

**Abstract:** Aqueous zinc-ion batteries are considered one of the promising large-scale energy storage devices of the future because of their high energy density, simple preparation process, efficient and safe discharge process, abundant zinc reserves, and low cost. However, the development of cathode materials with high capacity and stable structure has become one of the key elements to further development of aqueous zinc-ion batteries. Vanadium-based compounds, as one of the cathode materials for aqueous zinc-ion batteries, have various structures and high reversible capacities. Among them, vanadium-based sulfides have higher academic ability, better electrochemical activity, lower ion diffusion potential barrier, and a faster ion diffusion rate. As a result, vanadium-based sulfides have received extensive attention and research. In this review, we summarize the recent progress of vanadium-based sulfides applied in aqueous zinc-ion batteries, highlighting their effective strategies for designing optimized electrochemical performance and the underlying electrochemical mechanisms. Finally, an overview is provided of current vanadium-based sulfides and their prospects, and other perspectives on vanadium-based sulfide cathode materials for aqueous zinc-ion batteries are also discussed.

**Keywords:** vanadium sulfides; cathode materials; zinc-ion batteries; energy storage mechanisms



**Citation:** Hu, E.; Li, H.; Zhang, Y.; Wang, X.; Liu, Z. Recent Progresses on Vanadium Sulfide Cathodes for Aqueous Zinc-Ion Batteries. *Energies* **2023**, *16*, 917. <https://doi.org/10.3390/en16020917>

Academic Editor: Carlos Miguel Costa

Received: 16 December 2022

Revised: 7 January 2023

Accepted: 11 January 2023

Published: 13 January 2023



**Copyright:** © 2023 by the authors. Licensee MDPI, Basel, Switzerland. This article is an open access article distributed under the terms and conditions of the Creative Commons Attribution (CC BY) license (<https://creativecommons.org/licenses/by/4.0/>).

## 1. Introduction

As traditional fossil fuels continue to deplete and due to the gradual increase in the greenhouse effect, there are growing concerns about energy scarcity and environmental issues [1–3]. It has become an essential strategy for sustainable development to vigorously develop and replace traditional fossil fuels with reliable, clean, renewable energy. However, wind, solar, and tidal energy, which are constrained by natural conditions, have insufficient effective utilization to support their application in energy storage systems on a large scale. Therefore, it is indispensable to develop new energy conversion and storage systems with high efficiency, low cost, stability, and safety [4–6]. Lithium-ion batteries are one of the most widely used electrochemical energy storage systems in commercial applications due to their high energy density, long cycle life, and proven preparation processes. They are attempting to be incorporated into a wide range of power grids in the near future. However, lithium-ion batteries are expensive to manufacture due to the limited global resources of lithium metal. In addition, environmental pollution caused by using organic electrolytes seriously hinders their further development and large-scale application [7–9].

Therefore, research workers have turned their attention to secondary aqueous metal-ion batteries, which are abundant in reserves and environmentally friendly [10,11]. Among many aqueous metal-ion batteries, aqueous zinc-ion batteries (AZIBs) have received extensive research for their low cost, high safety, simple fabrication process, high theoretical capacity of  $820 \text{ mAh} \cdot \text{g}^{-1}$  ( $\sim 5855 \text{ mAh} \cdot \text{cm}^{-3}$ ) of the zinc metal anode, low redox potential of  $-0.76 \text{ V}$  (vs.  $\sim \text{SHE}$ ), high stability, etc., all unique advantages that make these batteries widely studied [12–19]. With the development of AZIBs, it has been widely

studied that manganese-based compounds, vanadium-based compounds, and Prussian blue analogs can be used as zinc-ion battery cathodes [20]. Manganese-based compounds ( $\text{MnO}_2$ ) [21–23] and vanadium-based oxides ( $\text{V}_2\text{O}_5$ ) cannot meet the ideal practical requirements due to their unstable crystal structures and poor cycling performance [24], while Prussian blue analogs [ $\text{Zn}_3(\text{Fe}(\text{CN})_6)_2$ ] have small capacities ( $\sim \pm 50 \text{ mAh} \cdot \text{g}^{-1}$ ) that hinder their practical applications, although their crystal structures are stable [20,25–27]. Therefore, developing cathode materials with stable crystal structures and excellent cycling stability is essential to promoting the development of aqueous Zn-ion batteries [28–32].

Based on the variable valence (standard valence states of +2, +3, +4, and +5) and the active nature of the vanadium element, it can carry out multiple electronic transfer redox reactions and thus exhibits a high capacity [25,28,33,34]. Vanadium-based sulfide nanomaterials, due to their unique structure, abundant redox activity, fast ion diffusion kinetics, and low ion diffusion potential, determine them to be a good choice as materials for zinc-ion batteries with aqueous cathodes [35–39]. Figure 1 shows typical types of vanadium-based sulfides and describes the advantages and disadvantages of vanadium-based sulfides for use in aqueous zinc-ion batteries. As the chemical composition and valence of vanadium changes, it allows vanadium atoms to combine with sulfur atoms to exhibit a diverse range of material species, as well as exhibit diverse structures such as layered structure ( $\text{VS}_2$ ), chain-like structure ( $\text{VS}_4$ ), and tunnel structure ( $\text{V}_5\text{S}_8$ ), which also determine the various properties of vanadium-based sulfides. Currently, the investigation of V-based sulfides is still at a relatively early stage. There are no articles that review and analyze the recent progress of vanadium-based sulfides as AZIB cathodes. In this review, we summarize recent developments in vanadium-based sulfides as cathode materials for AZIBs, highlighting the mechanisms of zinc-ion storage in the materials and effective ways to optimize electrochemical performance. Finally, some reasonable insights into the current challenges and future applications of vanadium-based sulfides are presented, which may shed light on the research and development of new high-performance vanadium-based sulfide cathode materials for AZIBs.

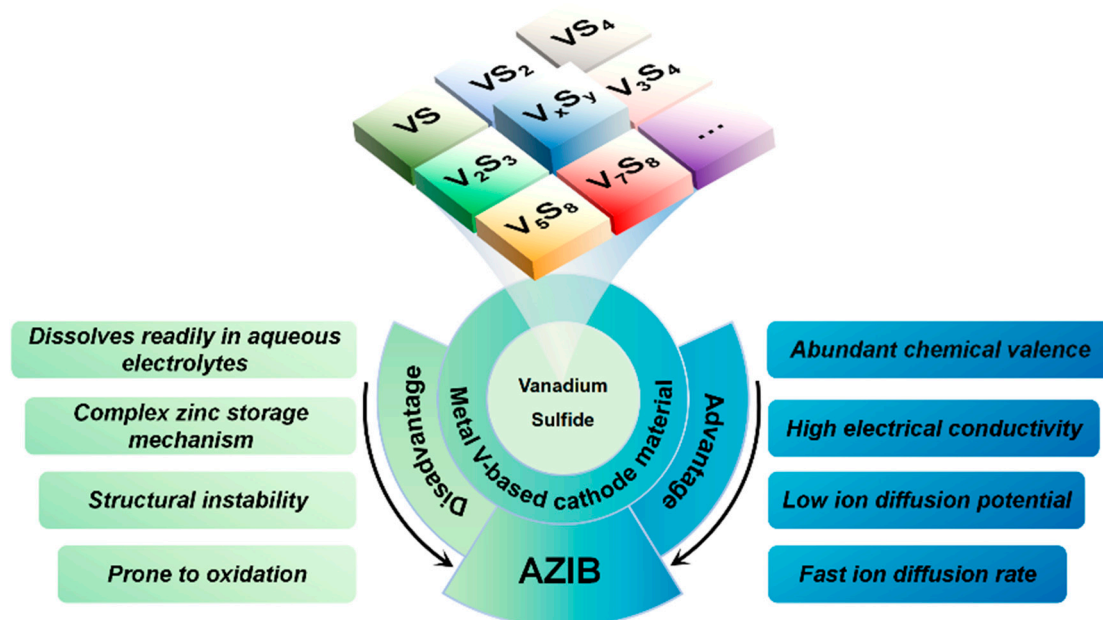


**Figure 1.** Types of vanadium-based sulfides and advantages and disadvantages of their application in aqueous zinc-ion batteries.

## 2. $\text{VS}_2$ and Its Composites in AZIBs

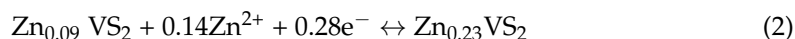
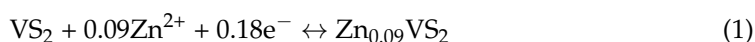
Two-dimensional layered transition metal disulfides (TMDs) have the structural formula  $\text{MX}_2$ , where M represents transition metal elements, including titanium, vanadium, molybdenum, tungsten, and tantalum, and X represents sulfur group elements, including

sulfur, selenium, etc. Based on their unique two-dimensional layered crystal structure and diverse chemical composition, they are not only beneficial as ion transport carriers to accommodate the volume changes during ion insertion but also make these materials have wonderful optoelectronic properties that can be widely used for energy conversion and harvesting [37,40–43].

VS<sub>2</sub>, one of the most common types of TMDs, has a typical two-dimensional layered crystal structure composed of an open sandwich structure of S-V-S, with adjacent layers bonded together by weak van der Waals forces with a layer spacing of 5.76 Å. The large layer spacing also facilitates the insertion/withdrawal of monovalent metal ions (Li<sup>+</sup>~0.69 Å, Na<sup>+</sup>~1.02 Å) and multivalent metal ions (Zn<sup>2+</sup>~0.74 Å, Mg<sup>2+</sup>~1.32 Å), thus enabling fast ion diffusion [44,45]. In addition, in the VS<sub>2</sub> crystal structure, each V atom is surrounded by six sulfur atoms and connected by covalent bonds to S atoms, which belong to the hexagonal crystal system. The advantages of VS<sub>2</sub>, such as good metallic properties, high conductivity (~5.0 × 10<sup>2</sup> S·m<sup>−1</sup>), and faster ion diffusion rate than 2D layered graphene, make VS<sub>2</sub> widely studied and applied as a novel cathode material [46].

Mai's team [47] prepared VS<sub>2</sub> nanosheets with thicknesses of 50–100 nm by a simple one-step hydrothermal method and used them for the first time as a cathode material for AZIBs (Figure 2a,b). Subsequently, metallic zinc was used as the anode, a weakly acidic salt solution (ZnSO<sub>4</sub>) as the electrolyte, and glass fibers as the isolator (Figure 2c). In the voltage interval of 0.4–1.0 V, the nanosheets exhibited a high reversible capacity of 190.3 mAh·g<sup>−1</sup> at 0.05 A·g<sup>−1</sup> at current density. As of 200 cycles with a current density of 0.5 A·g<sup>−1</sup>, the capacity retention rate was 98.0%, demonstrating that VS<sub>2</sub> has long-term cycling stability as a cathode material for AZIBs. As shown in Figure 1d, they investigated the storage mechanism of the Zn/VS<sub>2</sub> system during charging and discharging by non-in situ XRD tests. As the discharge process proceeded, the intensity of the characteristic peak located at 15.4° (001) gradually decreased slightly, and its position shifted to the left, which was caused by the interlayer spacing of the insertion of Zn<sup>2+</sup> into the crystal plane of (001) being enlarged during the discharge process. Instead, when fully charged, the intensity and position of the characteristic peaks of the (001) crystal plane return to the initial state due to the extraction of Zn<sup>2+</sup> during the charging process, as shown by the ex situ XRD results of the structural evolution being fully reversible during the discharge/charging process. In addition, in situ Raman, ex situ SAED, ex situ XPS, and ex situ HRTEM tests also demonstrated the reversibility of the structure evolution, which is consistent with ex situ XRD results. The following is a summary of the electrochemical reaction between Zn/VS<sub>2</sub> electrodes.

In the cathode:



In the cathode:



However, as a result of structural instability during charging and discharging, VS<sub>2</sub> cathode materials have been seriously hindered in their development [37]. The Du team [48] constructed fluffy and porous VS<sub>2</sub>/VO<sub>x</sub> cathode materials by in situ electrochemical pre-treatment (first charging to 1.8 V) (Figure 2e–i), taking advantage of the chemical instability of VS<sub>2</sub> in aqueous electrolytes. Because of the internal electric field of the heterogeneous interface, the high conductivity of VS<sub>2</sub>, and the high chemical stability of VO<sub>x</sub> (V<sub>6</sub>O<sub>13</sub>/VO<sub>2</sub>/V<sub>2</sub>O<sub>5</sub>), the average working potential of VS<sub>2</sub>/VO<sub>x</sub> with a heterogeneous structure is increased by 0.25 V. A high current density of 10.0 A g<sup>−1</sup> produces a high capacity of 156 mAh g<sup>−1</sup> at voltages between 0.2 and 1.8 V, with a capacity retention rate of 75% at a high current density of 1 A g<sup>−1</sup> after 3000 cycles. In addition, Figure 2j illustrates the VS<sub>2</sub>/VO<sub>x</sub> shift of the diffraction peak of VS<sub>2</sub>/V<sub>6</sub>O<sub>13</sub>/V<sub>2</sub>O<sub>5</sub> in ex situ XRD, proving the process of Zn<sup>2+</sup> de-intercalation.

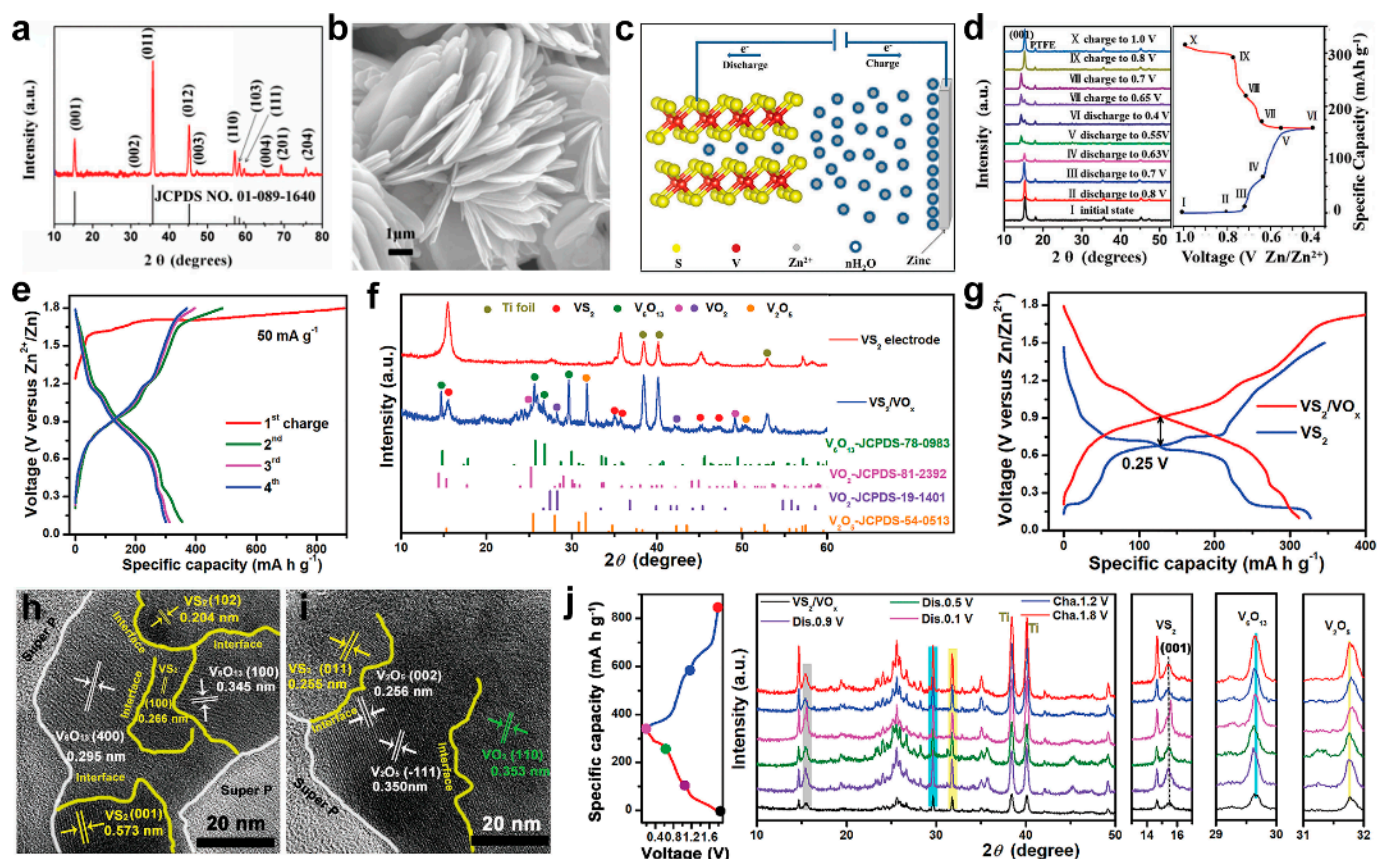


**Figure 2.** (a) The XRD of layered VS<sub>2</sub> [47]. (b) The SEM of layered VS<sub>2</sub> [47]. (c) Schematic illustration of the operation mechanism of Zn/VS<sub>2</sub> AZIB [47]. (d) Ex situ XRD patterns of layered VS<sub>2</sub> [47]. (e) Electrostatic charging and discharging curves for VS<sub>2</sub> [48]. (f) Ex situ XRD patterns of the electrode at different charge states (SOC) [48]. (g) The average potential of VS<sub>2</sub> and VS<sub>2</sub>/VO<sub>x</sub> under the GCD curve in the second cycle [48]. (h,i) The HRTEM images of in situ formed VS<sub>2</sub>/VO<sub>x</sub> [48]. (j) Ex situ XRD patterns of VS<sub>2</sub>/VO<sub>x</sub> [48].

In addition to in situ electrochemical oxidation, with the in-depth study of VS<sub>2</sub>, Jiao's team [49] used glucose as a template to prepare 1T-VS<sub>2</sub> nanospheres by a one-step hydrothermal method (Figure 3a,b). It strengthened the layered structure of VS<sub>2</sub> by simply modulating the charge cut-off voltage, which allowed a part of Zn<sup>2+</sup> to reside in the interlayer as zinc pillars during repeated insertion/extraction. The 1T-VS<sub>2</sub> nanospheres with abundant active sites and stable layered structure facilitate the penetration of the aqueous electrolyte and ensure rapid electron/ion transfer, resulting in excellent rate performance and an ultra-long cycle life of the material in AZIBs. These nanospheres demonstrated excellent reversible capacities of 212.9 and 102.1 mAh·g<sup>-1</sup> at current densities of 0.1 and 0.5 A·g<sup>-1</sup>, respectively, in the voltage range of 0.4–0.85 V. At a current density of 2 A·g<sup>-1</sup> and 2000 cycles, the capacity retention was 86.7%. As shown in Figure 3c,d, the results by ex situ XRD indicate that the shift in the diffraction peak of (001) indicates the existence of an electron/ion reversible insertion/desertion process. When charged to 1.0 V, the (001) diffraction peak completely returns to its original position, compared to 0.85 V, where the (001) diffraction peak is still on the left side of the original position, indicating that some Zn<sup>2+</sup> is still present in the interlayer of VS<sub>2</sub>. The results of ex situ XPS, ex situ HRTEM, and ex situ EDX are consistent with ex situ XRD results (Figure 3e–i). In contrast, in the voltage range of 0.4–1.0 V, the “dead Zn<sup>2+</sup>” residing in the VS<sub>2</sub> nanospheres can completely separate from the layers due to the large charging cutoff voltage. With the charge and discharge cycle, the 1T-VS<sub>2</sub> nanospheres are prone to structural collapse. As a result, the



electrochemical performance of the material at 1.0 V is decreased compared with that at 0.85 V (Figure 3j).

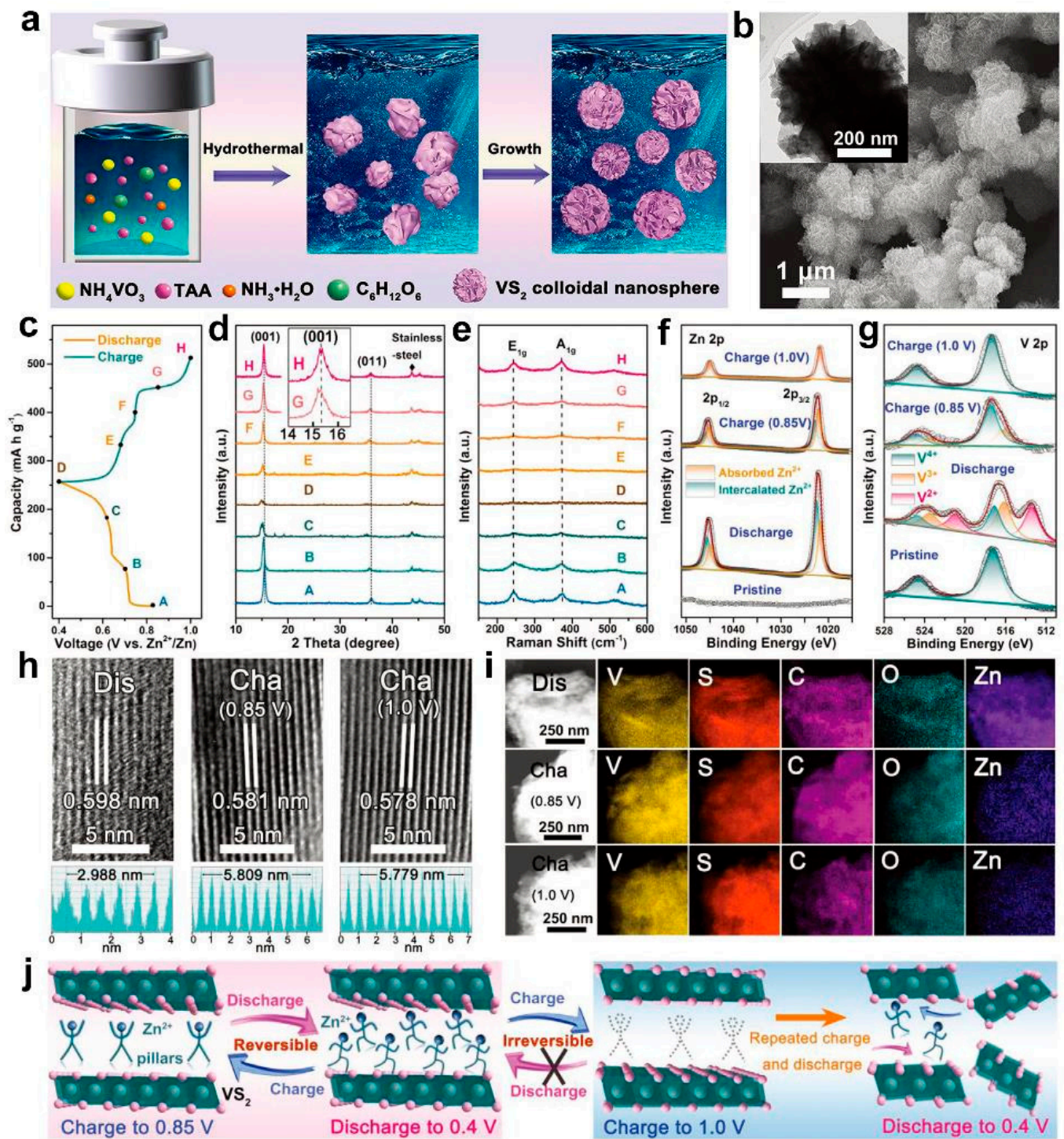


**Figure 3.** (a) Diagrammatic representation of the 1T-VS<sub>2</sub> growth process [49]. (b) The SEM and TEM images of 1T-VS<sub>2</sub> [49]. (c) 1T-VS<sub>2</sub> in the voltage range 0.4–1.0 V, GCD at different potential points in the first cycle (The coloured letters A–H in subfigures (c–e) indicate the different potential points) [49]. Ex-situ (d) XRD patterns of 1T-VS<sub>2</sub>, (e) Raman spectra of 1T-VS<sub>2</sub>, (f) Zn 2p, and (g) V 2p XPS spectra of 1T-VS<sub>2</sub>. (h) HRTEM images and (i) STEM element mapping images of the 1T-VS<sub>2</sub> [49]. (j) Diagram of the zinc-ion storage mechanism of 1T-VS<sub>2</sub> at different cut-off voltages (0.85 and 1.0 V) [49].

Binders are generally electrochemically inert substances, and their presence reduces the specific gravity of the active material of cathode materials; developing binder-free cathode materials is a new idea to enhance the specific capacity of batteries [50–53]. To solve this problem, the composite method of cathode material and carbon-based material can not only enhance the material's overall conductivity, promote the electrochemical reaction kinetics, and improve the rate performance, but also effectively alleviate the instability of the layered structure of  $\text{VS}_2$ . Wang's team [54] prepared rose-like nanoflowers composed of  $\text{VS}_2$  nanosheets by a simple one-step hydrothermal method, and by vacuum filtration after ultrasonication in a DMF solution C- $\text{VS}_2$  thin films were prepared (Figure 4a,b). The electrode films prepared by chemical bond integration under binder-free conditions enhance the interaction forces and provide fast electron transfer kinetics. In the voltage interval of 0.3–1.5 V, the composite films exhibited high specific capacities of 205.3 and 135.4  $\text{mAh}\cdot\text{g}^{-1}$  and excellent rate performance at the current densities of 0.1 and 10.0  $\text{A}\cdot\text{g}^{-1}$ , respectively, and at current densities of 0.5 and 5  $\text{A}\cdot\text{g}^{-1}$  capacity retention rates of 90% and 72% after 200 and 1500 cycles, respectively. In addition, the high percentage of the active material of the cathode material and the high electrical and mechanical conductivity of the SWCNTs also make the C- $\text{VS}_2$  film highly conductive and flexible, so that the soft-pack battery composed of C- $\text{VS}_2$  film exhibits stable electrochemical performance under different bending states. When the bending radii of the soft-pack battery are 2.0 cm and 1.0 cm, the discharge capacities of the device are 129.6  $\text{mAh}\cdot\text{g}^{-1}$  in the 40th cycle and 127.5  $\text{mAh}\cdot\text{g}^{-1}$  in the 61st cycle (Figure 4c,d illustrate that only 2.1  $\text{mAh}\cdot\text{g}^{-1}$  of battery discharge capacity was lost following the bending test).

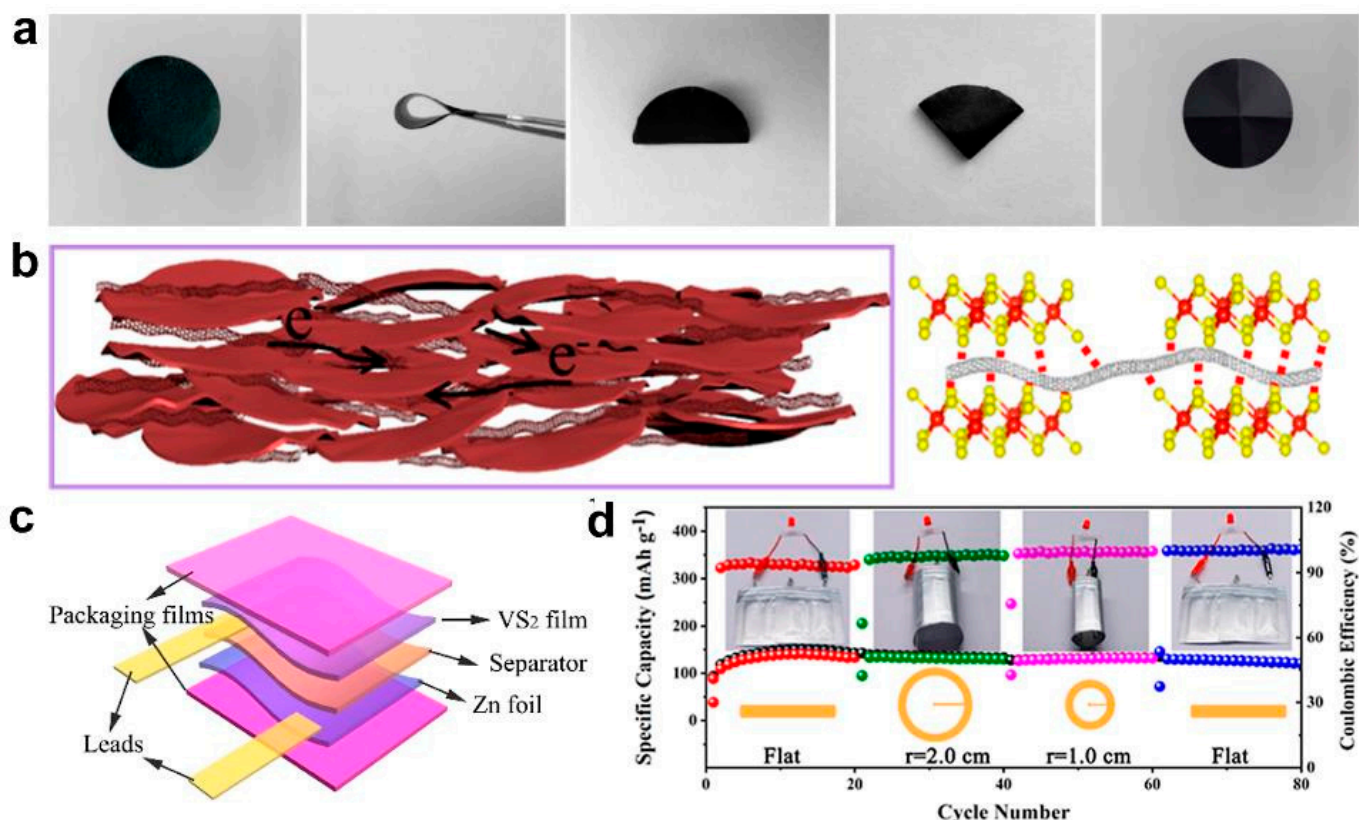


**Figure 4.** (a) Optical images of the flexible C- $\text{VS}_2$  film [54]. (b) Diagram of C- $\text{VS}_2$  composite achieving C-V chemical bond independence [54]. (c) Soft-packaged Zn//C- $\text{VS}_2$  battery schematic diagram [54]. (d) Cycle performance of flexible packaging battery in different bending states ( $0.5 \text{ A}\cdot\text{g}^{-1}$ ) and LED screen lighting in different bending states [54].

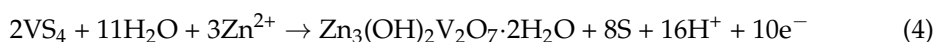


### 3. VS<sub>4</sub> and Its Composites in AZIBs

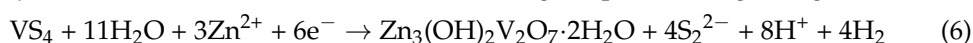
VS<sub>4</sub> was first discovered in the Whinstone mineral, and its crystal structure was elucidated in 1964 and has been widely studied in recent years as an AZIB cathode material with high performance [55–57].

The crystal structure of VS<sub>4</sub> is a one-dimensional “linear atomic chain” compound consisting of V<sup>4+</sup> with two sulfur dimers (S<sub>2</sub><sup>2−</sup>)<sub>2</sub> coordinated along the c-axis; Figure 5a shows the results [58]. Each VS<sub>4</sub> atomic chain is held together by weak van der Waals forces between the bond, and the spacing between the atomic chains is 5.83 Å [59], which is significantly larger than the effective ionic diameter of Zn<sup>2+</sup> (0.74 Å) [16]. There are plenty of active sites for Zn<sup>2+</sup> storage and diffusion between the open channels between the atomic chains.

However, an electrochemical reaction’s kinetics are affected by the poor electron/ion conductivity of VS<sub>4</sub>, and this makes electrode materials challenging to meet high-performance requirements [60–62]. Wang’s team [63] prepared VS<sub>4</sub>@rGO nanomaterials with a simple hydrothermal method and used them as high-performance positive electrode materials for AZIBs (Figure 5b). The use of rGO with superior electrical conductivity as the conductive substrate [60,64,65] improves the electrical conductivity of the VS<sub>4</sub>@rGO composite, enabling the electrode material to maintain a capacity retention rate of 93.3% while providing a high capacity of 180 mAh·g<sup>−1</sup> after 200 cycles at a current density of 1 A·g<sup>−1</sup>. Additionally, the reaction process is accompanied by the formation of Zn<sub>3</sub>(OH)<sub>2</sub>V<sub>2</sub>O<sub>7</sub>·2H<sub>2</sub>O and sulfur, per the ex situ XRD data (Figure 5c), and with the reversible shift of the (011) crystal plane also suggests a reversible insertion/extraction reaction mechanism of Zn<sup>2+</sup>:



Similarly, Sun’s team [66] used a one-step hydrothermal method to prepare nano-flower-like VS<sub>4</sub>/CNT cathode materials with a rich mesoporous structure (Figure 5d), which increased the contact area with the electrolyte, shortened the diffusion distance of Zn<sup>2+</sup>, and improved the electron transport capacity of the cathode. High reversible capacities of 265 and 182 mAh·g<sup>−1</sup> were provided at current densities of 0.25 and 7 A·g<sup>−1</sup>, respectively, and it has a 93% capacity retention rate after 1200 cycles at a current density of 5 A·g<sup>−1</sup>. As shown in Figure 5e,f, the charge/discharge cycle in the first turn is significantly different from the subsequent charge/discharge cycles, indicating the occurrence of a phase transition in the first turn. Based on ex situ XRD and XPS, the mechanism of the phase change reaction of VS<sub>4</sub> during the first cycle and the reversible intercalation of Zn<sup>2+</sup> during the subsequent cycles are described (Figure 5g–i). In the first discharge process (1D 1.0~0.2 V), the characteristic peak of VS<sub>4</sub> gradually weakened, and the crystalline phase of ZVO (Zn<sub>3</sub>(OH)<sub>2</sub>V<sub>2</sub>O<sub>7</sub>·2H<sub>2</sub>O) and monomeric S appeared. During the following charging process, the characteristic peak of ZVO still exists, and the characteristic peak of the resulting monomeric sulfur disappears as it is dissolved in the electrolyte. As shown in Figure 4j, the relevant reaction mechanisms following the phase change are given:



The acidic conditions are as follows:



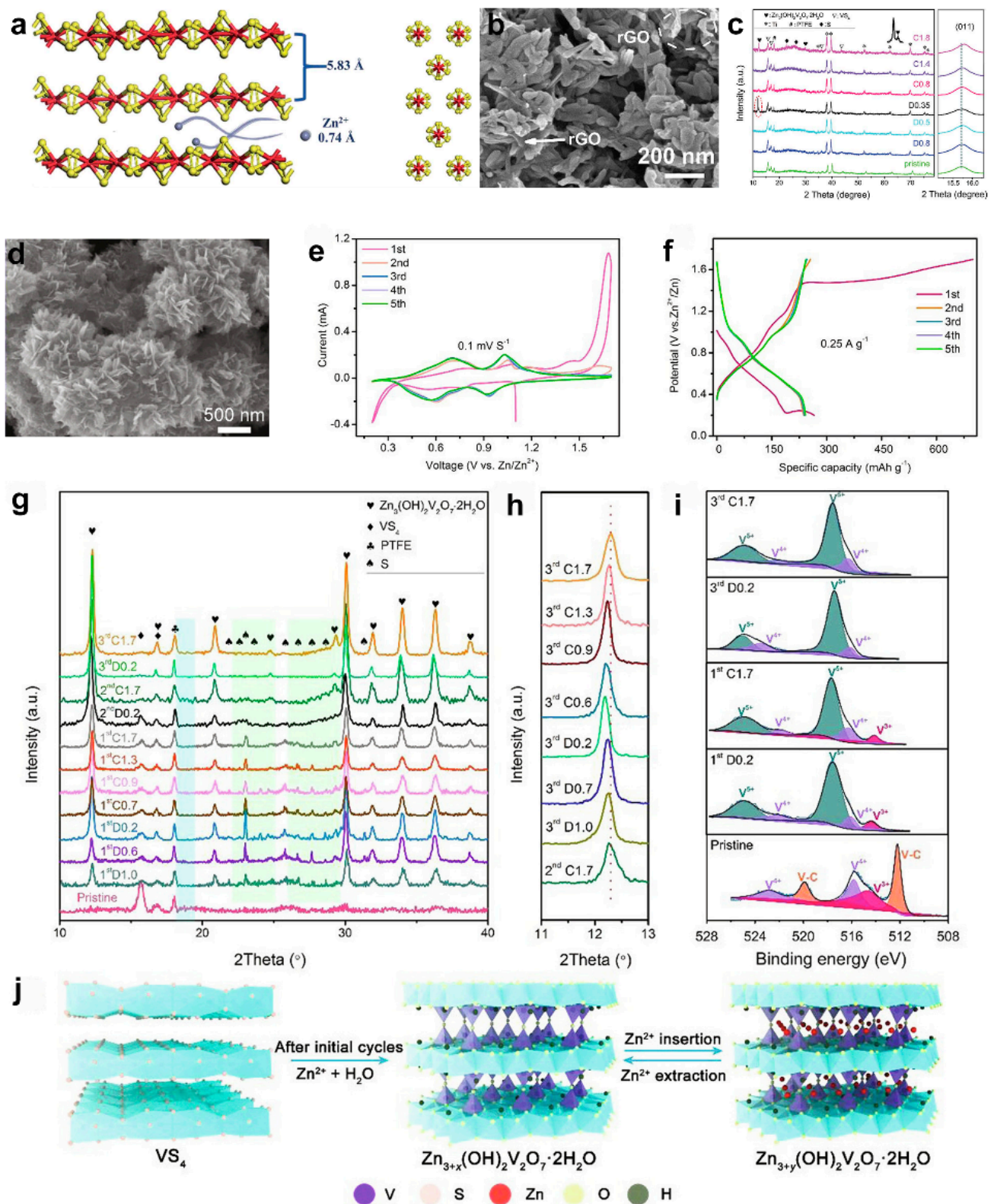


**Figure 5.** (a) Schematic diagram of the VS<sub>4</sub> [58]. (b) The SEM image of VS<sub>4</sub>@rGO [63]. (c) Ex situ XRD patterns of VS<sub>4</sub>@rGO in the first charge/discharge cycle [63]. (d) The SEM images of VS<sub>4</sub>/CNTs. (e) CV curves of VS<sub>4</sub>/CNTs electrode at a scan rate of 0.1 mV·s<sup>-1</sup> [66]. (f) Discharge-charge profiles of VS<sub>4</sub>/CNTs electrode at 0.25 A·g<sup>-1</sup> [66]. Ex situ (g) XRD patterns of VS<sub>4</sub>/CNTs, (h) enlarged area of ZVO (001) planes, and (i) V 2p XPS spectra of VS<sub>4</sub>/CNT [66]. (j) Schematic representation of the reaction mechanism of the VS<sub>4</sub>/CNT cathode during cycling [66].



In order to further improve zinc-ion storage capacity, the construction of heterogeneous structures with sufficient interfaces and grain boundaries is a highly promising and effective strategy. Cheng's team [67] used as a proof of concept the oxidation of  $\text{VS}_4$  prepared by a one-step hydrothermal method to a  $\text{VS}_4/\text{V}_2\text{O}_3$  heterostructure in a tube furnace after depilatory oxidation in contact with an external source of oxygen. Concomitantly, by comparing with the precursor  $\text{VS}_4$  and the fully converted product  $\text{V}_2\text{O}_3$ , the  $\text{VS}_4/\text{V}_2\text{O}_3$  heterostructure has a higher zinc-ion storage capacity, providing a capacity of  $163 \text{ mAh}\cdot\text{g}^{-1}$  at a current density of  $0.1 \text{ A}\cdot\text{g}^{-1}$  in the voltage range of 0.3–1.2 V, which is much higher than that of  $\text{VS}_4$  ( $47 \text{ mAh}\cdot\text{g}^{-1}$ ) and  $\text{V}_2\text{O}_3$  ( $74 \text{ mAh}\cdot\text{g}^{-1}$ ) in the same voltage range.

Similarly, Du's team [68] again used an in situ electrochemically induced phase transition method (the same method used to prepare  $\text{VS}_2/\text{VO}_x$  heterostructures) to prepare  $\text{S}/\text{VO}_x$  composites by simple in situ electrochemical oxidation using  $\text{VS}_4$  as a precursor. The initial discharge capacity of  $376 \text{ mAh}\cdot\text{g}^{-1}$  was provided at a current density of  $0.05 \text{ A}\cdot\text{g}^{-1}$  in the voltage range of 0.1–1.8 V, and  $260 \text{ mAh}\cdot\text{g}^{-1}$  at a current density of  $2 \text{ A}\cdot\text{g}^{-1}$ , with 100% capacity retention after 2000 cycles, demonstrating the excellent rate performance and ultra-long cycle life of the composites. Combined with ex situ XRD, a reversible insertion and removal of  $\text{Zn}^{2+}$  after phase transition has been demonstrated as an energy storage mechanism.

#### 4. Other Vanadium Sulfides and Their Composites in AZIBs

Due to their chemical stability, variety of crystal structures, and high electrical conductivity, intermediate transition metal–sulfur compounds (TMDCs) are frequently utilized as cathode materials in metal-ion battery systems [41]. However, when repeated cycling is performed on layered TMDC materials, the high polarization of zinc ions can result in structural collapse and severe anisotropic diffusion, leading to a weakened zinc-ion intercalation efficiency and reduced electrical resistance [15,38,49,69,70]. These intrinsic shortcomings are a serious impediment to further developing stable, high-rate, layered TMDCs as cathode materials. The solution to these issues lies in designing TMDCs with tunnel-like structures or unique NiAs structures, which is a potentially effective strategy.

##### 4.1. $\text{V}_5\text{S}_8$

Zhu's team [71] developed a  $\text{V}_5\text{S}_8$  cathode material with a tunnel-like structure and applied it to AZIBs for the first time. By a simple calcination method, depletion in an Ar atmosphere caused the dimeric  $\text{S}_2^{2-}$  to monomeric  $\text{S}^{2-}$  transformation in  $\text{VS}_4$ , thus facilitating the phase transition from one-dimensional chained  $\text{VS}_4$  to tunneled  $\text{V}_5\text{S}_8$  (Figure 6a,b). Due to ordered vacancies in a NiAs-type structure, vanadium atoms in  $\text{V}_5\text{S}_8$  partially occupy one-fourth of the available S-S octahedral sites between two adjacent  $\text{VS}_2$  monolayers. This creates multiple ion paths that enable quick and reversible de-embedding of zinc ions while ensuring structural and electrochemical property stability. As a result, the  $\text{V}_5\text{S}_8$  cathode material provides a high specific capacity of  $240 \text{ mAh}\cdot\text{g}^{-1}$  at a current density of  $0.1 \text{ A}\cdot\text{g}^{-1}$ , exhibits an excellent rate performance of  $193.8 \text{ mAh}\cdot\text{g}^{-1}$  at a current density of  $10 \text{ A}\cdot\text{g}^{-1}$ , and has a capacity retention rate of 94% after 1000 cycles. In addition, as shown in Figure 6c,d,  $\text{V}_5\text{S}_8$  exhibits stronger metallic properties, lower hopping energy barriers, and better Zn ion diffusion paths based on density flooding theory calculations (DFT). As shown in Figure 6e–h, sequential and reversible  $\text{H}^+$ ,  $\text{Zn}^{2+}$  de/intercalation reaction mechanisms are also proposed based on in situ XRD and ex situ XPS characterization:

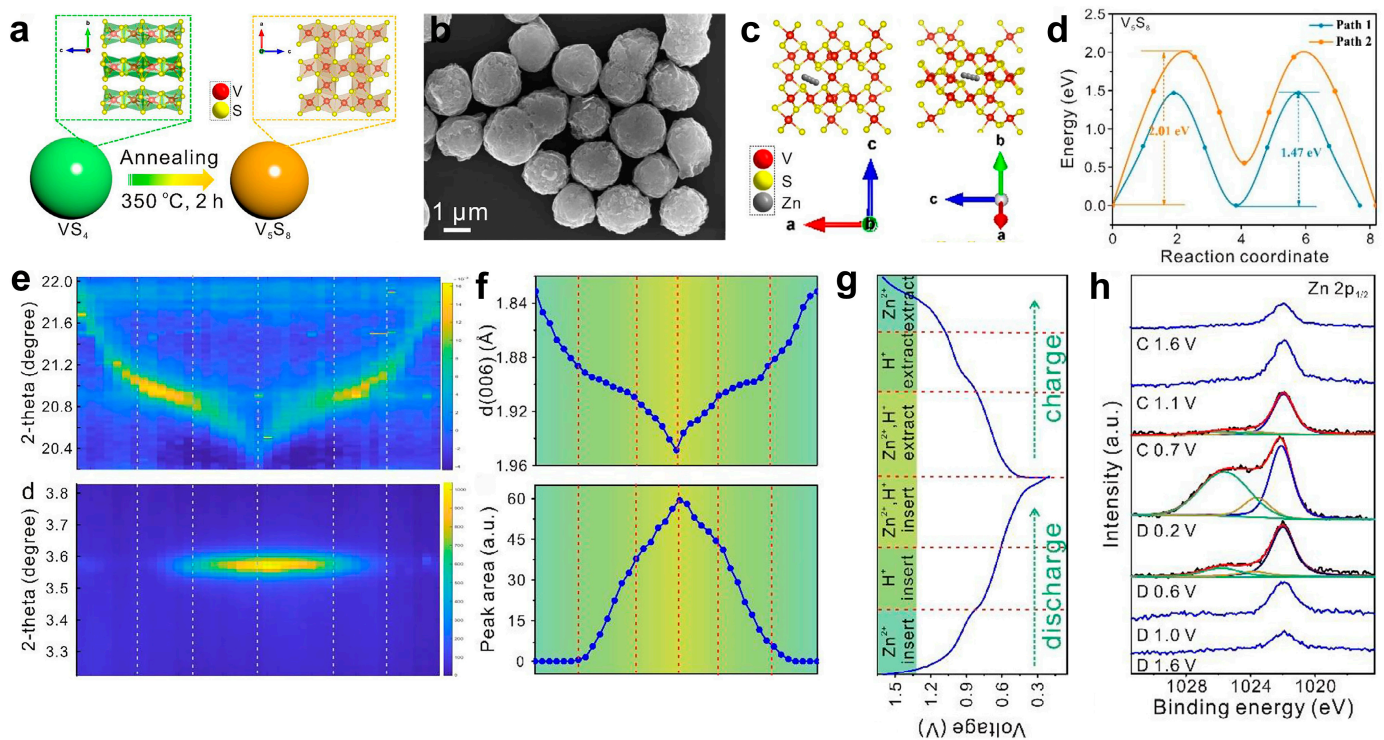
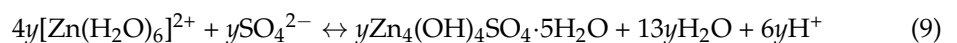
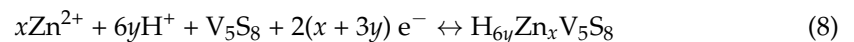
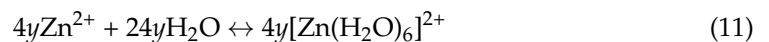
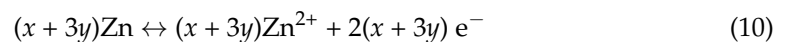


**Figure 6.** (a) Diagram of the preparation process of  $V_5S_8$  [71]. (b) The SEM images of  $V_5S_8$  [71]. (c) Schematic diagram of the diffusion pathway of Zn atoms in the  $V_5S_8$  anode (path I and II) [71]. (d) The corresponding diffusion energy barrier curves for different paths in  $V_5S_8$  [71]. (e) In situ SXR patterns of the  $V_5S_8$  (006) characteristic peak and  $V_5S_8$  (001) characteristic peak [71]. (f) Changes in the interlayer spacing of the crystalline surfaces associated with  $V_5S_8$  during discharge/charging and the corresponding peak area of the side reaction product  $Zn_4SO_4(OH)_6 \cdot 5H_2O$  [71]. (g) Discharge/charging curves in the voltage range of 0.2–1.6 V during the in situ observation [71]. (h) Ex situ XPS spectra of Zn 2p at selected states [71].

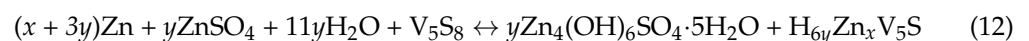
Cathode:



Anode:

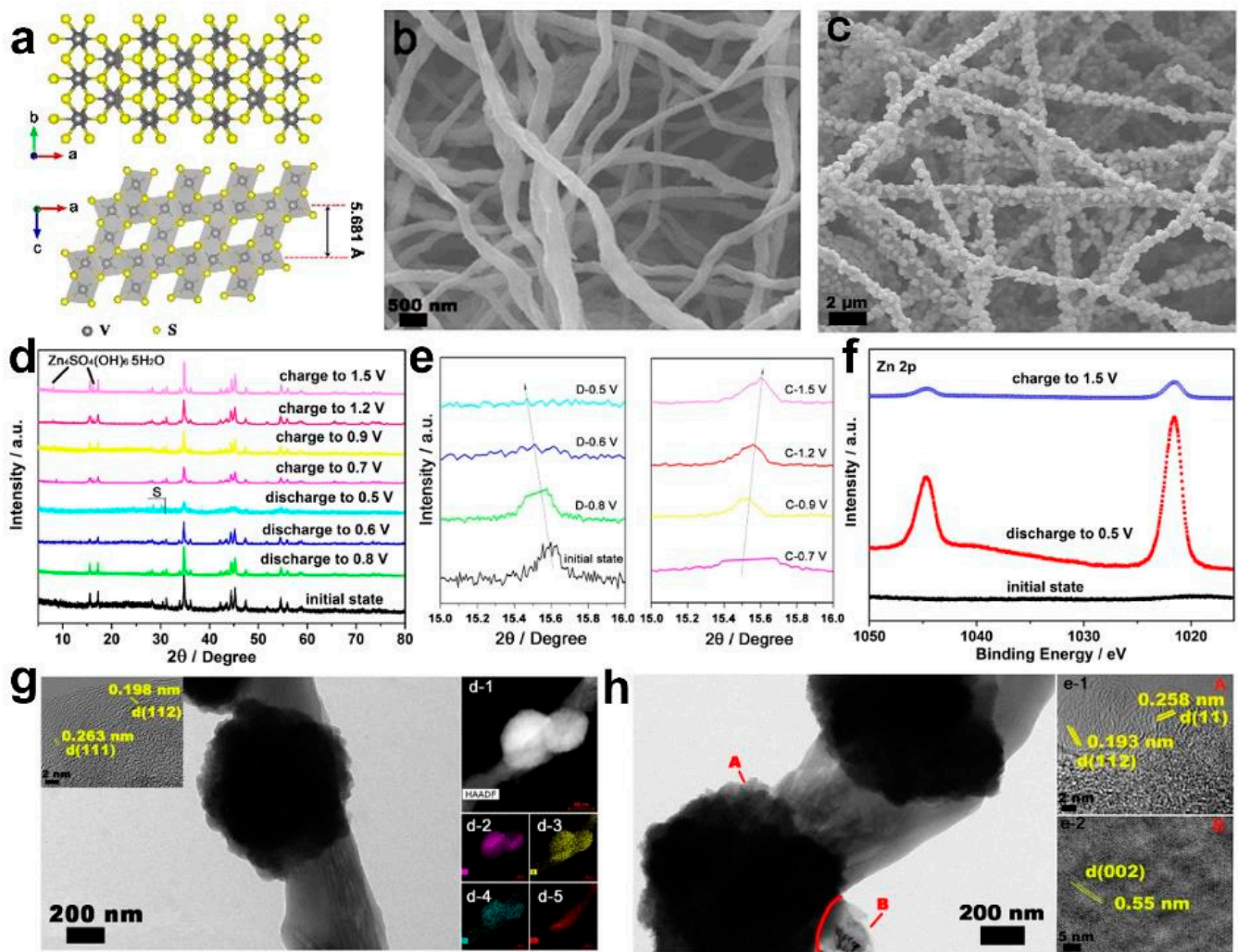


Overall:



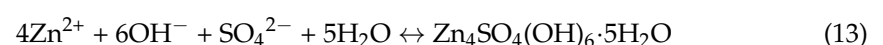
#### 4.2. $V_3S_4$

An essential member of the vanadium sulfide family, as shown in Figure 7a,  $V_3S_4$ , with its unique NiAs type, usually occurs as  $V_{0.5}VS_2$  (consisting of a  $VS_2$  monomolecular layer and a 0.5V atom linking two adjacent layers). In this structure, due to the intense contact between the  $V^{3+}$  and  $V^{4+}$  cations, the intercalated V atoms ( $V^{3+}$ ) exhibit metallic conduction along the c-axis direction, which should aid in the transmission of electrons along their c-axis path [72–77].



**Figure 7.** (a) Schematic diagram of the  $V_3S_4$  [78]. (b) The SEM images of the HCC and (c) the HCC- $V_3S_4$  [78]. Ex situ (d,e) XRD patterns of HCC- $V_3S_4$  and (f) XPS spectra of HCC- $V_3S_4$  [78]. (g) TEM and HRTEM diagrams of the HCC- $V_3S_4$  electrodes after discharge to 0.5 V and (h) charging to 1.5 V [78].

Pan's team [78] developed a composite cathode material with a NiAs-type structure of  $V_3S_4$ . As shown in Figure 7b,c, the material was first prepared by electrostatic spinning and calcination of a new composite flexible carbon matrix (a novel composite flexible substrate containing acidified halloysite, carbon fibers, and carbon nanotubes) with high electrical conductivity and strong hydrophilicity, followed by a one-step hydrothermal method to obtain nanospherical  $V_3S_4$  attached to the filamentary new composite flexible carbon matrix, which was applied to flexible AZIBs. The composite cathode material HCC- $V_3S_4$  has a high specific capacity of  $148 \text{ mAh} \cdot \text{g}^{-1}$  after 200 cycles at a current density of  $0.5 \text{ A} \cdot \text{g}^{-1}$  and a specific capacity of  $102 \text{ mAh} \cdot \text{g}^{-1}$  after 1000 cycles at a current density of  $5 \text{ A} \cdot \text{g}^{-1}$  in the voltage range of 0.5–1.5 V. This design of loading nanomaterials onto conductive carbon substrates promotes electron transfer and avoids using conductive agents and binders, thus improving electrochemical properties. The energy storage device's carbon substrate's increased surface hydrophilicity also enhances the composite's electrochemical characteristics. In addition, the energy storage mechanism of the HCC- $V_3S_4$  cathode was investigated by a series of non-in situ characterizations, as shown in Figure 7d–h. In addition, the reaction expression is proposed for  $Zn_4SO_4(OH)_6 \cdot 5H_2O$  generated during the charging process:

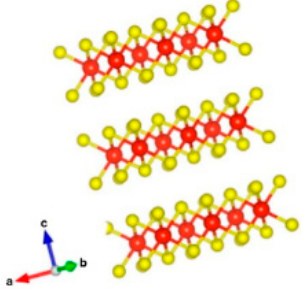
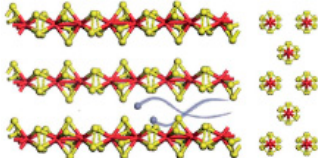
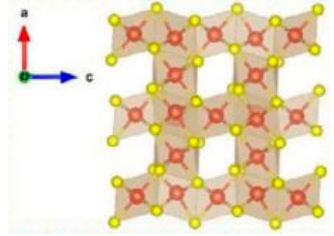
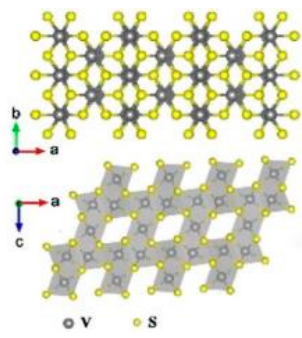




## 5. Summary and Outlook

AZIBs, as new green and environmentally friendly secondary batteries, are widely studied for their low production cost, high safety, simple preparation process, and environmental friendliness, and are expected to be widely used in areas such as large-scale energy storage and electronic devices. As an extremely promising cathode material for AZIBs, vanadium-based sulfides show great potential for development in AZIBs due to their low development costs, diverse material combinations, rich crystal structures (layer, chain, and tunnel), and valence changes ( $V^{2+}$ ,  $V^{3+}$ ,  $V^{4+}$ , and  $V^{5+}$ ). Table 1 summarizes the structure and reaction mechanisms of different types of vanadium sulfides in AZIBs.

**Table 1.** Summary of the structure and mechanism of vanadium sulfide cathode materials in AZIBs.

Types of Vanadium Sulfides	Crystal Structure Models	Interplanar Crystal Spacing (Å)	Reaction Mechanisms	Ref.
$VS_2$		5.76	Interlayer mechanism	[50]
$VS_4$		5.83	Transformation/ interlayer mechanism	[58]
$V_5S_8$		11.32	Interlayer mechanism	[71]
$V_3S_4$		5.681	Interlayer mechanism	[78]

In this review, we provide an overview of recent research advances in vanadium-based sulfide and their composites as cathode materials for aqueous zinc-ion batteries and highlight their various design strategies and the structural characteristics and energy storage mechanisms of the materials, providing some insights into the design of new high-performance cathode materials for AZIBs and facilitating the practical application of AZIBs. The main direction of the application of vanadium-based sulfides in AZIBs is their use

as cathode materials. Figure 8 and Table 2 summarize the timeline and electrochemical performance of vanadium-based sulfides and their composites as cathode materials for aqueous zinc-ion batteries. In addition, there is a lack of investigation into more directions on ZIBs for vanadium-based sulfides (e.g., electrolytes, separator, anode protection, etc.), which may be a significant direction for future research. Although vanadium-based sulfides have made tremendous progress as positive electrode materials for AZIBs, these materials are currently immature for practical applications, and their further development still faces several challenges, such as typically lower operating voltage, easier dissolution in aqueous electrolytes, easier structural collapse during cycling, and more complex zinc storage mechanisms. Meanwhile, according to the defects of vanadium-based sulfides as AZIBs cathode materials, the following optimization strategies are proposed: (1) acting as pillars by embedding metal ions, etc., which can effectively reinforce the material structure; (2) using carbon materials as the substrate to improve the conductivity of the material; (3) in situ electrochemical activations to build heterogeneous structures, which can promote the rapid intercalation of ions and alleviate the volume expansion during cycling; (4) developing binder-free cathode materials, which can improve the overall conductivity of the material, promote the kinetics of electrochemical reactions, and effectively enhance the multiplier performance. In summary, the development of integrated cathode materials with stable structure, higher ionic/electronic conductivity, abundant active sites, and easy  $\text{Zn}^{2+}$  de/intercalation between layers is the key to realizing the wide application of AZIBs.

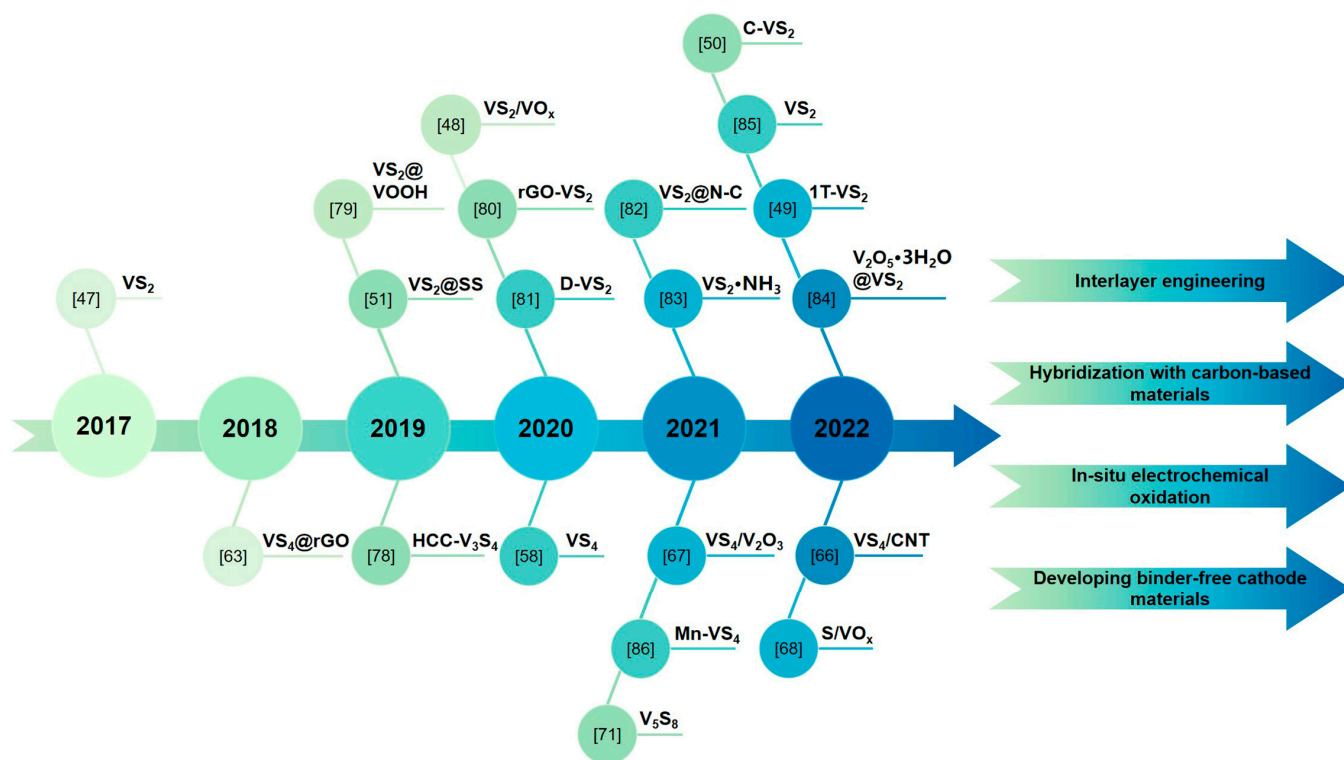


**Figure 8.** Timeline for the development of vanadium-based sulfides as cathode materials for AZIBs.

**Table 2.** Summary of electrochemical performance of vanadium sulfide cathode materials in AZIBs.

Cathode Material	Electrolyte	Voltage Range (V)	Capacity ( $\text{mAh}\cdot\text{g}^{-1}@\text{A}\cdot\text{g}^{-1}$ )	Cycle Stability	Ref.
$\text{VS}_2$	1 M $\text{ZnSO}_4$	0.4–1.0	190.3@0.05	98% after 200 cycles at $0.5\text{ A}\cdot\text{g}^{-1}$	[47]
$\text{VS}_2@\text{VOOH}$	3 M $\text{ZnSO}_4$	0.4–1.0	184.2@0.05	82% after 400 cycles at $2.5\text{ A}\cdot\text{g}^{-1}$	[79]

Table 2. Cont.

Cathode Material	Electrolyte	Voltage Range (V)	Capacity (mAh·g <sup>-1</sup> @A g <sup>-1</sup> )	Cycle Stability	Ref.
VS <sub>2</sub> @SS	1 M ZnSO <sub>4</sub>	0.4–1.0	98@0.05	80% after 1600 cycles at 1.0 A g <sup>-1</sup>	[50]
rGO-VS <sub>2</sub>	3 M Zn (CF <sub>3</sub> SO <sub>3</sub> ) <sub>2</sub>	0.2–1.8	238@0.1	93% after 1000 cycles at 5.0 A g <sup>-1</sup>	[80]
D-VS <sub>2</sub>	1 M ZnSO <sub>4</sub>	0.2–1.7	262@0.1	94% after 100 cycles at 0.1 A g <sup>-1</sup>	[81]
VS <sub>2</sub> @N-C	3 M Zn (CF <sub>3</sub> SO <sub>3</sub> ) <sub>2</sub>	0.2–1.8	203@0.05	97% after 600 cycles at 1.0 A g <sup>-1</sup>	[82]
VS <sub>2</sub> ·NH <sub>3</sub>	2 M Zn (CF <sub>3</sub> SO <sub>3</sub> ) <sub>2</sub>	0.2–1.7	392@0.1	110% after 2000 cycles at 3.0 A g <sup>-1</sup>	[83]
VS <sub>2</sub> /VO <sub>x</sub>	25 M ZnCl <sub>2</sub>	0.1–1.8	301@0.05	75% after 3000 cycles at 1.0 A g <sup>-1</sup>	[48]
V <sub>2</sub> O <sub>5</sub> ·3H <sub>2</sub> O@VS <sub>2</sub> (SVO)	3 M ZnSO <sub>4</sub>	0.3–1.6	290@0.5	69.7% after 6700 cycles at 5.0 A g <sup>-1</sup>	[84]
VS <sub>2</sub>	1 M ZnSO <sub>4</sub>	0.2–1.0	450.7@0.1	72% after 200 cycles at 1.0 A g <sup>-1</sup>	[85]
1T-VS <sub>2</sub>	2.5 M Zn (CF <sub>3</sub> SO <sub>3</sub> ) <sub>2</sub>	0.4–0.85	212.9@0.1	86.7% after 2000 cycles at 2.0 A g <sup>-1</sup>	[49]
VS <sub>2</sub> @SWCNT(C-VS <sub>2</sub> )	3 M Zn (CF <sub>3</sub> SO <sub>3</sub> ) <sub>2</sub>	0.3–1.5	205.3@0.1	72% after 1500 cycles at 5.0 A g <sup>-1</sup>	[54]
VS <sub>4</sub> @rGO	1 M Zn (CF <sub>3</sub> SO <sub>3</sub> ) <sub>2</sub>	0.35–1.8	180@1.0	93.3% after 165 cycles at 1.0 A g <sup>-1</sup>	[63]
VS <sub>4</sub>	1 M ZnSO <sub>4</sub>	0.2–1.6	310@0.1	85% after 500 cycles at 2.5 A g <sup>-1</sup>	[58]
VS <sub>4</sub> /CNTs	2 M Zn (CF <sub>3</sub> SO <sub>3</sub> ) <sub>2</sub>	0.2–1.7	265@0.25	93% after 1200 cycles at 5.0 A g <sup>-1</sup>	[66]
S/VO <sub>x</sub>	30 M ZnCl <sub>2</sub>	0.1–1.8	376@0.05	100% after 2000 cycles at 2.0 A g <sup>-1</sup>	[68]
VS <sub>4</sub> /V <sub>2</sub> O <sub>3</sub>	3 M Zn (CF <sub>3</sub> SO <sub>3</sub> ) <sub>2</sub>	0.3–1.2	163@0.1	-	[67]
Mn-VS <sub>4</sub>	1 M Zn (CF <sub>3</sub> SO <sub>3</sub> ) <sub>2</sub> / ACN (1:1)	0.3–2.0 V	547@0.1	97.83% after 1000 cycles at 1.0 A g <sup>-1</sup>	[86]
V <sub>5</sub> S <sub>8</sub>	3 M ZnSO <sub>4</sub>	0.2–1.6	240@0.1	94% after 1000 cycles at 10.0 A g <sup>-1</sup>	[71]
HCC-V <sub>3</sub> S <sub>4</sub>	2 M ZnSO <sub>4</sub>	0.5–1.5	148@0.5	95% after 200 cycles at 0.5 A g <sup>-1</sup>	[78]

**Funding:** This work was supported by the National Natural Science Foundation of China (Grant Nos. 22005167 and 21905152), the Shandong Provincial Natural Science Foundation of China (Grant Nos. ZR2020QB125), the China Postdoctoral Science Foundation (Grant Nos. 2021M693256, 2021T140687 and 2022M713249), the Qingdao Postdoctoral Applied Research Project, the Taishan Scholar Project of Shandong Province of China (ts20190937), and the Youth Innovation Team Project for Talent Introduction and Cultivation in Universities of Shandong Province.

**Data Availability Statement:** Not applicable.

**Conflicts of Interest:** The authors declare no competing financial interest.

## References

1. Ao, H.; Zhao, Y.; Zhou, J.; Cai, W.; Zhang, X.; Zhu, Y.; Qian, Y. Rechargeable aqueous hybrid ion batteries: Developments and prospects. *J. Mater. Chem. A* **2019**, *7*, 18708–18734. [\[CrossRef\]](#)
2. Ling, J.; Kunwar, R.; Li, L.; Peng, S.; Misnon, I.I.; Ab Rahim, M.H.; Yang, C.-C.; Jose, R. Self-rechargeable energizers for sustainability. *eScience* **2022**, *2*, 347–364. [\[CrossRef\]](#)



3. Liu, Q.; Liu, R.; He, C.; Xia, C.; Guo, W.; Xu, Z.-L.; Xia, B. Advanced polymer-based electrolytes in zinc–air batteries. *eScience* **2022**, *2*, 453–466. [\[CrossRef\]](#)
4. Larcher, D.; Tarascon, J.M. Towards greener and more sustainable batteries for electrical energy storage. *Nat. Chem.* **2015**, *7*, 19–29. [\[CrossRef\]](#)
5. Wang, X.; Zhang, Z.; Xi, B.; Chen, W.; Jia, Y.; Feng, J.; Xiong, S. Advances and Perspectives of Cathode Storage Chemistry in Aqueous Zinc-Ion Batteries. *ACS Nano* **2021**, *15*, 9244–9272. [\[CrossRef\]](#)
6. Liu, Z.; Sun, H.; Wang, X.; Gu, Z.-Y.; Xu, C.; Li, H.; Zhang, G.; He, Y.; Wu, X.-L. Tetrafunctional template-assisted strategy to precisely construct co-doped Sb@C nanofiber with longitudinal tunnels for ultralong-life and high-rate sodium storage. *Energy Stor. Mater.* **2022**, *48*, 90–100. [\[CrossRef\]](#)
7. Yang, Y.; Bremner, S.; Menictas, C.; Kay, M. Battery energy storage system size determination in renewable energy systems: A review. *Renew. Sust. Energy Rev.* **2018**, *91*, 109–125. [\[CrossRef\]](#)
8. Tian, Y.; Zeng, G.; Rutt, A.; Shi, T.; Kim, H.; Wang, J.; Koettgen, J.; Sun, Y.; Ouyang, B.; Chen, T.; et al. Promises and Challenges of Next-Generation "Beyond Li-ion" Batteries for Electric Vehicles and Grid Decarbonization. *Chem. Rev.* **2021**, *121*, 1623–1669. [\[CrossRef\]](#)
9. Liu, Z.; Li, H.; He, Y.; Sun, H.; Xu, C.; Li, H.; Wang, X.; Zhang, G.; Sun, Z.; Wei, Q.; et al. An integrated strategy based on Schiff base reactions to construct unique two-dimensional nanostructures for intrinsic pseudocapacitive sodium/lithium storage. *Chem. Eng. J.* **2022**, *429*, 132339. [\[CrossRef\]](#)
10. Yan, H.; Zhang, X.; Yang, Z.; Xia, M.; Xu, C.; Liu, Y.; Yu, H.; Zhang, L.; Shu, J. Insight into the electrolyte strategies for aqueous zinc ion batteries. *Coord. Chem. Rev.* **2022**, *452*, 7517–7556. [\[CrossRef\]](#)
11. Wang, M.; Meng, Y.; Li, K.; Ahmad, T.; Chen, N.; Xu, Y.; Sun, J.; Chuai, M.; Zheng, X.; Yuan, Y.; et al. Toward dendrite-free and anti-corrosion Zn anodes by regulating a bismuth-based energizer. *eScience* **2022**, *2*, 509–517. [\[CrossRef\]](#)
12. Ruan, P.; Liang, S.; Lu, B.; Fan, H.J.; Zhou, J. Design Strategies for High-Energy-Density Aqueous Zinc Batteries. *Angew. Chem. Int. Ed. Engl.* **2022**, *61*, e202200598. [\[CrossRef\]](#)
13. Wang, H.; Ye, W.; Yang, Y.; Zhong, Y.; Hu, Y. Zn-ion hybrid supercapacitors: Achievements, challenges and future perspectives. *Nano Energy* **2021**, *85*, 105942. [\[CrossRef\]](#)
14. Zhang, F.; Liao, T.; Liu, C.; Peng, H.; Luo, W.; Yang, H.; Yan, C.; Sun, Z. Biomineralization-inspired dendrite-free Zn-electrode for long-term stable aqueous Zn-ion battery. *Nano Energy* **2022**, *103*, 107830. [\[CrossRef\]](#)
15. Song, M.; Tan, H.; Chao, D.; Fan, H.J. Recent Advances in Zn-Ion Batteries. *Adv. Funct. Mater.* **2018**, *28*, 1802564. [\[CrossRef\]](#)
16. Fang, G.; Zhou, J.; Pan, A.; Liang, S. Recent Advances in Aqueous Zinc-Ion Batteries. *ACS Energy Lett.* **2018**, *3*, 2480–2501. [\[CrossRef\]](#)
17. Zhang, Y.; Chen, A.; Sun, J. Promise and challenge of vanadium-based cathodes for aqueous zinc-ion batteries. *J. Energy Chem.* **2021**, *54*, 655–667. [\[CrossRef\]](#)
18. Wang, Z.; Zhou, M.; Qin, L.; Chen, M.; Chen, Z.; Guo, S.; Wang, L.; Fang, G.; Liang, S. Simultaneous regulation of cations and anions in an electrolyte for high-capacity, high-stability aqueous zinc–vanadium batteries. *eScience* **2022**, *2*, 209–218. [\[CrossRef\]](#)
19. Wang, X.; Li, Y.; Jin, T.; Meng, J.; Jiao, L.; Zhu, M.; Chen, J. Electrospun Thin-Walled CuCo<sub>2</sub>O<sub>4</sub>@C Nanotubes as Bifunctional Oxygen Electrocatalysts for Rechargeable Zn–Air Batteries. *Nano Lett.* **2017**, *17*, 7989–7994. [\[CrossRef\]](#)
20. Zhang, X.; Wang, L.; Fu, H. Recent advances in rechargeable Zn-based batteries. *J. Power Sources* **2021**, *493*, 229677. [\[CrossRef\]](#)
21. Hua, F.; Fan, M. Research progress on Mn based oxide as cathode material for ZIBs. *New Chem. Mater.* **2021**, *49*, 1006–3536.
22. Zhang, B.; Chen, J.; Sun, W.; Shao, Y.; Zhang, L.; Zhao, K. Challenges and Perspectives for Doping Strategy for Manganese-Based Zinc-ion Battery Cathode. *Energies* **2022**, *15*, 4698. [\[CrossRef\]](#)
23. Chuai, M.; Yang, J.; Wang, M.; Yuan, Y.; Liu, Z.; Xu, Y.; Yin, Y.; Sun, J.; Zheng, X.; Chen, N.; et al. High-performance Zn battery with transition metal ions co-regulated electrolytic MnO<sub>2</sub>. *eScience* **2021**, *1*, 178–185. [\[CrossRef\]](#)
24. Wang, L.; Zheng, J. Recent advances in cathode materials of rechargeable aqueous zinc-ion batteries. *Mater. Today Adv.* **2020**, *7*, 100078. [\[CrossRef\]](#)
25. Li, S.; Wei, X.; Chen, H.; Lai, G.; Wang, X.; Zhang, S.; Wu, S.; Tang, W.; Lin, Z. A mixed-valent vanadium oxide cathode with ultrahigh rate capability for aqueous zinc-ion batteries. *J. Mater. Chem. A* **2021**, *9*, 22392–22398. [\[CrossRef\]](#)
26. Tolstopyatova, E.G.; Kamenskii, M.A.; Kondratiev, V.V. Vanadium Oxide–Conducting Polymers Composite Cathodes for Aqueous Zinc-Ion Batteries: Interfacial Design and Enhancement of Electrochemical Performance. *Energies* **2022**, *15*, 8966. [\[CrossRef\]](#)
27. He, P.; Chen, Q.; Yan, M.; Xu, X.; Zhou, L.; Mai, L.; Nan, C.-W. Building better zinc-ion batteries: A materials perspective. *Energy Chem.* **2019**, *1*, 100022. [\[CrossRef\]](#)
28. Liang, Y.; Dong, H.; Aurbach, D.; Yao, Y. Current status and future directions of multivalent metal-ion batteries. *Nat. Energy* **2020**, *5*, 646–656. [\[CrossRef\]](#)
29. Blanc, L.E.; Kundu, D.; Nazar, L.F. Scientific Challenges for the Implementation of Zn-Ion Batteries. *Joule* **2020**, *4*, 771–799. [\[CrossRef\]](#)
30. Huang, J.; Li, Y.; Xie, R.; Li, J.; Tian, Z.; Chai, G.; Zhang, Y.; Lai, F.; He, G.; Liu, C.; et al. Structural engineering of cathodes for improved Zn-ion batteries. *J. Energy Chem.* **2021**, *58*, 147–155. [\[CrossRef\]](#)
31. Du, M.; Miao, Z.; Li, H.; Sang, Y.; Liu, H.; Wang, S. Strategies of structural and defect engineering for high-performance rechargeable aqueous zinc-ion batteries. *J. Mater. Chem. A* **2021**, *9*, 19245–19281. [\[CrossRef\]](#)

32. Tang, B.; Shan, L.; Liang, S.; Zhou, J. Issues and opportunities facing aqueous zinc-ion batteries. *Energy Environ. Sci.* **2019**, *12*, 3288–3304. [\[CrossRef\]](#)
33. Yi, T.-F.; Qiu, L.; Qu, J.-P.; Liu, H.; Zhang, J.-H.; Zhu, Y.-R. Towards high-performance cathodes: Design and energy storage mechanism of vanadium oxides-based materials for aqueous Zn-ion batteries. *Coord. Chem. Rev.* **2021**, *446*, 214124. [\[CrossRef\]](#)
34. Liu, H.; Wang, J.-G.; You, Z.; Wei, C.; Kang, F.; Wei, B. Rechargeable aqueous zinc-ion batteries: Mechanism, design strategies and future perspectives. *Mater. Today* **2021**, *42*, 73–98. [\[CrossRef\]](#)
35. Xiaoru, Y.; Yufang, C.; Peitao, X.; Chunman, Z. Review on Oxygen-Free Vanadium-Based Cathodes for Aqueous Zinc-Ion Batteries. *J. Electrochem.* **2022**, *28*, 2219004.
36. Xu, X.; Xiong, F.; Meng, J.; Wang, X.; Niu, C.; An, Q.; Mai, L. Vanadium-Based Nanomaterials: A Promising Family for Emerging Metal-Ion Batteries. *Adv. Funct.* **2020**, *30*, 1904398. [\[CrossRef\]](#)
37. Li, T.; Li, H.; Yuan, J.; Xia, Y.; Liu, Y.; Sun, A. Recent Advance and Modification Strategies of Transition Metal Dichalcogenides (TMDs) in Aqueous Zinc Ion Batteries. *Materials* **2022**, *15*, 2654. [\[CrossRef\]](#)
38. Liu, B. Transition Metal Dichalcogenides for High-Performance Aqueous Zinc Ion Batteries. *Batteries* **2022**, *8*, 62. [\[CrossRef\]](#)
39. Ding, J.; Gao, H.; Ji, D.; Zhao, K.; Wang, S.; Cheng, F. Vanadium-based cathodes for aqueous zinc-ion batteries: From crystal structures, diffusion channels to storage mechanisms. *J. Mater. Chem. A* **2021**, *9*, 5258–5275. [\[CrossRef\]](#)
40. Yun, Q.; Lu, Q.; Zhang, X.; Tan, C.; Zhang, H. Three-Dimensional Architectures Constructed from Transition-Metal Dichalcogenide Nanomaterials for Electrochemical Energy Storage and Conversion. *Angew. Chem. Int. Ed.* **2018**, *57*, 626–646. [\[CrossRef\]](#)
41. Lee, W.S.V.; Xiong, T.; Wang, X.; Xue, J. Unraveling MoS<sub>2</sub> and Transition Metal Dichalcogenides as Functional Zinc-Ion Battery Cathode: A Perspective. *Small Methods* **2021**, *5*, e2000815. [\[CrossRef\]](#) [\[PubMed\]](#)
42. Hoang Huy, V.P.; Ahn, Y.N.; Hur, J. Recent Advances in Transition Metal Dichalcogenide Cathode Materials for Aqueous Rechargeable Multivalent Metal-Ion Batteries. *Nanomaterials* **2021**, *11*, 1517. [\[CrossRef\]](#) [\[PubMed\]](#)
43. Wang, X.; Wei, Q.; Li, H.; Sun, J.; Li, H.; He, Y.; Liu, Z. Iron-chalcogenide-based electrode materials for electrochemical energy storage. *J. Mater. Chem. A* **2022**, *10*, 7517–7556. [\[CrossRef\]](#)
44. Wu, Y.; Song, T.-Y.; Chen, L.-N. A review on recent developments of vanadium-based cathode for rechargeable zinc-ion batteries. *Tungsten* **2021**, *3*, 289–304. [\[CrossRef\]](#)
45. Chen, X.; Zhang, H.; Liu, J.-H.; Gao, Y.; Cao, X.; Zhan, C.; Wang, Y.; Wang, S.; Chou, S.-L.; Dou, S.-X.; et al. Vanadium-based cathodes for aqueous zinc-ion batteries: Mechanism, design strategies and challenges. *Energy Stor. Mater.* **2022**, *50*, 21–46. [\[CrossRef\]](#)
46. Wan, F.; Niu, Z. Design Strategies for Vanadium-based Aqueous Zinc-Ion Batteries. *Angew. Chem. Int. Ed.* **2019**, *58*, 16358–16367. [\[CrossRef\]](#)
47. He, P.; Yan, M.; Zhang, G.; Sun, R.; Chen, L.; An, Q.; Mai, L. Layered VS<sub>2</sub> Nanosheet-Based Aqueous Zn Ion Battery Cathode. *Adv. Energy Mater.* **2017**, *7*, 1601920. [\[CrossRef\]](#)
48. Yu, D.; Wei, Z.; Zhang, X.; Zeng, Y.; Wang, C.; Chen, G.; Shen, Z.X.; Du, F. Boosting Zn<sup>2+</sup> and NH<sub>4</sub><sup>+</sup> Storage in Aqueous Media via In-Situ Electrochemical Induced VS<sub>2</sub>/VO<sub>x</sub> Heterostructures. *Adv. Funct. Mater.* **2020**, *31*, 2008743. [\[CrossRef\]](#)
49. Tan, Y.; Li, S.W.; Zhao, X.D.; Wang, Y.; Shen, Q.Y.; Qu, X.H.; Liu, Y.C.; Jiao, L.F. Unexpected Role of the Interlayer "Dead Zn<sup>2+</sup>" in Strengthening the Nanostructures of VS<sub>2</sub> Cathodes for High-Performance Aqueous Zn-Ion Storage. *Adv. Energy Mater.* **2022**, *12*, 2104001. [\[CrossRef\]](#)
50. Jiao, T.; Yang, Q.; Wu, S.; Wang, Z.; Chen, D.; Shen, D.; Liu, B.; Cheng, J.; Li, H.; Ma, L.; et al. Binder-free hierarchical VS<sub>2</sub> electrodes for high-performance aqueous Zn ion batteries towards commercial level mass loading. *J. Mater. Chem. A* **2019**, *7*, 16330–16338. [\[CrossRef\]](#)
51. Feng, M.; Wang, W.; Hu, Z.; Fan, C.; Zhao, X.; Wang, P.; Li, H.; Yang, L.; Wang, X.; Liu, Z. Engineering chemical-bonded Ti<sub>3</sub>C<sub>2</sub> MXene@carbon composite films with 3D transportation channels for promoting lithium-ion storage in hybrid capacitors. *Sci. China Mater.* **2022**, 1248. [\[CrossRef\]](#)
52. Wang, W.; Feng, M.; Hu, E.; Hu, Z.; Fan, C.; Li, H.; Wang, P.; Wang, X.; Liu, Z. Interlayer and intralayer co-modified flexible V<sub>2</sub>CT<sub>x</sub> MXene@SWCNT films for high-power Li-ion capacitors. *J. Energy Chem.* **2022**, *22*, 2095–4956. [\[CrossRef\]](#)
53. Wang, X.; Wang, R.; Zhao, Z.; Bi, S.; Niu, Z. Controllable spatial engineering of flexible all-in-one graphene-based supercapacitors with various architectures. *Energy Stor. Mater.* **2019**, *23*, 269–276. [\[CrossRef\]](#)
54. Sun, H.; Yang, L.; Hu, E.; Feng, M.; Fan, C.; Wang, W.; Li, H.; Wang, X.; Liu, Z. Rose-like VS<sub>2</sub> Nanosheets Chemically Anchored on Carbon Nanotubes for Flexible Zinc-Ion Batteries with Enhanced Properties. *ACS Appl. Mater. Interfaces* **2022**, *14*, 40247–40256. [\[CrossRef\]](#)
55. Yao, K.; Wu, M.; Chen, D.; Liu, C.; Xu, C.; Yang, D.; Yao, H.; Liu, L.; Zheng, Y.; Rui, X. Vanadium Tetrasulfide for Next-Generation Rechargeable Batteries: Advances and Challenges. *Chem. Rec.* **2022**, *22*, e202200117. [\[CrossRef\]](#)
56. Allmann, R.; Baumann, I.; Kutoglu, A.; Rösch, H.; Hellner, E. Die Kristallstruktur des Patronits V(S<sub>2</sub>)<sub>2</sub>. *Naturwissenschaften* **1964**, *51*, 263–264. [\[CrossRef\]](#)
57. Hillebrand, W.F. The Vanadium Sulphide, Patronite, and its Mineral Associates from Minasragra, Peru. *J. Am. Chem. Soc.* **1907**, *29*, 1019–1029. [\[CrossRef\]](#)
58. Zhu, Q.; Xiao, Q.; Zhang, B.; Yan, Z.; Liu, X.; Chen, S.; Ren, Z.; Yu, Y. VS<sub>4</sub> with a chain crystal structure used as an intercalation cathode for aqueous Zn-ion batteries. *J. Mater. Chem. A* **2020**, *8*, 10761–10766. [\[CrossRef\]](#)

59. Wang, Y.; Liu, Z.; Wang, C.; Yi, X.; Chen, R.; Ma, L.; Hu, Y.; Zhu, G.; Chen, T.; Tie, Z.; et al. Highly Branched VS<sub>4</sub> Nanodendrites with 1D Atomic-Chain Structure as a Promising Cathode Material for Long-Cycling Magnesium Batteries. *Adv. Mater.* **2018**, *30*, e1802563. [\[CrossRef\]](#)
60. Shen, C.; Li, X.; Li, N.; Xie, K.; Wang, J.G.; Liu, X.; Wei, B. Graphene-Boosted, High-Performance Aqueous Zn-Ion Battery. *ACS Appl. Mater. Interfaces* **2018**, *10*, 25446–25453. [\[CrossRef\]](#)
61. Ruan, P.; Xu, X.; Feng, J.; Yu, L.; Gao, X.; Shi, W.; Wu, F.; Liu, W.; Zang, X.; Ma, F.; et al. Boosting zinc storage performance via conductive materials. *Mater. Res. Bull.* **2021**, *133*, 111077. [\[CrossRef\]](#)
62. Zhang, T.; Zhang, L.; Hou, Y. MXenes: Synthesis strategies and lithium-sulfur battery applications. *eScience* **2022**, *2*, 164–182. [\[CrossRef\]](#)
63. Qin, H.; Yang, Z.; Chen, L.; Chen, X.; Wang, L. A high-rate aqueous rechargeable zinc ion battery based on the VS<sub>4</sub>@rGO nanocomposite. *J. Mater. Chem. A* **2018**, *6*, 23757–23765. [\[CrossRef\]](#)
64. Wang, X.; Liu, L.; Niu, Z. Carbon-based materials for lithium-ion capacitors. *Mater. Chem. Front.* **2019**, *3*, 1265–1279. [\[CrossRef\]](#)
65. Xu, C.; Wei, Q.; Li, M.; You, J.; Song, W.; Wang, X.; Zhang, G.; Li, H.; He, Y.; Liu, Z. Ultrafast and simple integration engineering of graphene-based flexible films with extensive tunability and simple trial in lithium-ion batteries. *J. Alloys Compd.* **2022**, *922*, 166282. [\[CrossRef\]](#)
66. Gao, S.; Ju, P.; Liu, Z.; Zhai, L.; Liu, W.; Zhang, X.; Zhou, Y.; Dong, C.; Jiang, F.; Sun, J. Electrochemically induced phase transition in a nanoflower vanadium tetrasulfide cathode for high-performance zinc-ion batteries. *J. Energy Chem.* **2022**, *69*, 356–362. [\[CrossRef\]](#)
67. Ding, J.; Gao, H.; Liu, W.; Wang, S.; Wu, S.; Fang, S.; Cheng, F. Operando constructing vanadium tetrasulfide-based heterostructures enabled by extrinsic adsorbed oxygen for enhanced zinc ion storage. *J. Mater. Chem. A* **2021**, *9*, 11433–11441. [\[CrossRef\]](#)
68. Deng, L.; Yu, D.; Sun, G.; Zhang, X.; Wang, C.; Tian, R.; Du, F. In-situ electrochemical synthesis of a high-performance S/VOx composite for aqueous zinc ion batteries. *J. Phys. D Appl. Phys.* **2022**, *55*, 274001. [\[CrossRef\]](#)
69. Wang, X.; Wang, F.; Wang, L.; Li, M.; Wang, Y.; Chen, B.; Zhu, Y.; Fu, L.; Zha, L.; Zhang, L.; et al. An Aqueous Rechargeable Zn/Co<sub>3</sub>O<sub>4</sub> Battery with High Energy Density and Good Cycling Behavior. *Adv. Mater.* **2016**, *28*, 4904–4911. [\[CrossRef\]](#)
70. Li, Y.; Fu, J.; Zhong, C.; Wu, T.; Chen, Z.; Hu, W.; Amine, K.; Lu, J. Recent Advances in Flexible Zinc-Based Rechargeable Batteries. *Adv. Energy Mater.* **2018**, *9*, 1802605. [\[CrossRef\]](#)
71. Ren, Z.; Sun, Y.; Yin, Y.; Zhang, J.; Ren, X.; Zhao, Y.; Liang, Z.; Huai, P.; Song, F.; Jiang, Z.; et al. Metallic V<sub>5</sub>S<sub>8</sub> microparticles with tunnel-like structure for high-rate and stable zinc-ion energy storage. *Energy Stor. Mater.* **2021**, *42*, 786–793. [\[CrossRef\]](#)
72. Tan, Z.; Liu, S.; Zhang, X.; Wei, J.; Liu, Y.; Hou, L.; Yuan, C. Few-layered V<sub>2</sub>C MXene derived 3D V<sub>3</sub>S<sub>4</sub> nanocrystal functionalized carbon flakes boosting polysulfide adsorption and catalytic conversion towards Li-S batteries. *J. Mater. Chem. A* **2022**, *10*, 18679–18689. [\[CrossRef\]](#)
73. Yao, G.; Niu, P.; Li, Z.; Xu, Y.; Wei, L.; Niu, H.; Yang, Y.; Zheng, F.; Chen, Q. Construction of flexible V<sub>3</sub>S<sub>4</sub>@CNF films as long-term stable anodes for sodium-ion batteries. *Chem. Eng. J.* **2021**, *423*, 130229. [\[CrossRef\]](#)
74. Wu, D.; Zhang, W.; Feng, Y.; Ma, J. Necklace-like carbon nanofibers encapsulating V<sub>3</sub>S<sub>4</sub> microspheres for ultrafast and stable potassium-ion storage. *J. Mater. Chem. A* **2020**, *8*, 2618–2626. [\[CrossRef\]](#)
75. Zhong, Y.; Chai, S.; Huang, X.; Zhou, S.; He, Q.; Lu, R.; Su, Q.; Pan, A. Hierarchical 1D/2D V<sub>3</sub>S<sub>4</sub>@N, S-Codoped rGO Hybrids as High-Performance Anode Materials for Fast and Stable Lithium-Ion Storage. *ACS Appl. Energy Mater.* **2022**, *5*, 4722–4732. [\[CrossRef\]](#)
76. Zhang, Y.; Li, J.; Ma, L.; Li, H.; Xu, X.; Liu, X.; Lu, T.; Pan, L. Insights into the storage mechanism of 3D nanoflower-like V<sub>3</sub>S<sub>4</sub> anode in sodium-ion batteries. *Chem. Eng. J.* **2022**, *427*, 130936. [\[CrossRef\]](#)
77. Zhang, H.; Zhang, Y.; Meng, Y.; Xiao, M.; Hu, J.; Zhao, G.; Liu, S.; Zhu, F. Composite V<sub>3</sub>S<sub>4</sub>@rGO nanowires as a high-performance anode material for lithium-/sodium-ion batteries. *Ionics* **2021**, *27*, 5067–5077. [\[CrossRef\]](#)
78. Liu, S.; Chen, X.; Zhang, Q.; Zhou, J.; Cai, Z.; Pan, A. Fabrication of an Inexpensive Hydrophilic Bridge on a Carbon Substrate and Loading Vanadium Sulfides for Flexible Aqueous Zinc-Ion Batteries. *ACS Appl. Mater. Interfaces* **2019**, *11*, 36676–36684. [\[CrossRef\]](#)
79. Pu, X.; Song, T.; Tang, L.; Tao, Y.; Cao, T.; Xu, Q.; Liu, H.; Wang, Y.; Xia, Y. Rose-like vanadium disulfide coated by hydrophilic hydroxyvanadium oxide with improved electrochemical performance as cathode material for aqueous zinc-ion batteries. *J. Power Sources* **2019**, *437*, 226917. [\[CrossRef\]](#)
80. Chen, T.; Zhu, X.; Chen, X.; Zhang, Q.; Li, Y.; Peng, W.; Zhang, F.; Fan, X. VS<sub>2</sub> nanosheets vertically grown on graphene as high-performance cathodes for aqueous zinc-ion batteries. *J. Power Sources* **2020**, *477*, 228652. [\[CrossRef\]](#)
81. Yin, B.-S.; Zhang, S.-W.; Xiong, T.; Shi, W.; Ke, K.; Lee, W.S.V.; Xue, J.; Wang, Z.-B. Engineering sulphur vacancy in VS<sub>2</sub> as high performing zinc-ion batteries with high cyclic stability. *New J. Chem.* **2020**, *44*, 15951–15957. [\[CrossRef\]](#)
82. Liu, J.; Peng, W.; Li, Y.; Zhang, F.; Fan, X. A VS<sub>2</sub>@N-doped carbon hybrid with strong interfacial interaction for high-performance rechargeable aqueous Zn-ion batteries. *J. Mater. Chem. C* **2021**, *9*, 6308–6315. [\[CrossRef\]](#)
83. Yang, M.; Wang, Z.; Ben, H.; Zhao, M.; Luo, J.; Chen, D.; Lu, Z.; Wang, L.; Liu, C. Boosting the zinc ion storage capacity and cycling stability of interlayer-expanded vanadium disulfide through in-situ electrochemical oxidation strategy. *J. Colloid Interface Sci.* **2022**, *607*, 68–75. [\[CrossRef\]](#)
84. Gao, P.; Pan, Z.; Ru, Q.; Zhang, J.; Zheng, M.; Zhao, X.; Ling, F.C.-C.; Wei, L. Synergetic V<sub>2</sub>O<sub>5</sub>·3H<sub>2</sub>O/Metallic VS<sub>2</sub> Nanocomposites Endow a Long Life and High Rate Capability to Aqueous Zinc-Ion Batteries. *Energy Fuels* **2022**, *36*, 3319–3327. [\[CrossRef\]](#)



85. Xu, J.; Liu, Y.; Chen, P.; Wang, A.; Huang, K.J.; Fang, L.; Wu, X. Interlayer-expanded VS<sub>2</sub> nanosheet: Fast ion transport, dynamic mechanism and application in Zn<sup>2+</sup> and Mg<sup>2+</sup>/Li<sup>+</sup> hybrid batteries systems. *J. Colloid Interface Sci.* **2022**, *620*, 119–126. [[CrossRef](#)] [[PubMed](#)]
86. Samanta, P.; Ghosh, S.; Jang, W.; Yang, C.-M.; Murmu, N.C.; Kuila, T. A Reversible Anodizing Strategy in a Hybrid Electrolyte Zn-Ion Battery through Structural Modification of a Vanadium Sulfide Cathode. *ACS Appl. Energy Mater.* **2021**, *4*, 10656–10667. [[CrossRef](#)]

**Disclaimer/Publisher's Note:** The statements, opinions and data contained in all publications are solely those of the individual author(s) and contributor(s) and not of MDPI and/or the editor(s). MDPI and/or the editor(s) disclaim responsibility for any injury to people or property resulting from any ideas, methods, instructions or products referred to in the content.